Supporting Information

Masters et al. 10.1073/pnas.1301766110

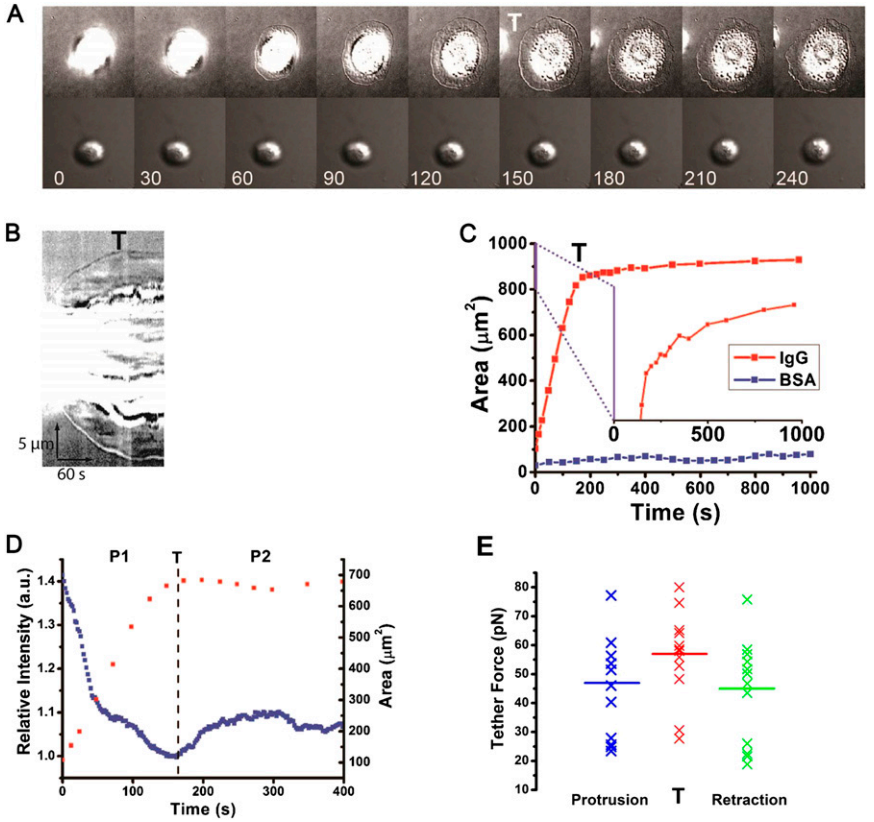

Fig. S1. Macrophage pseudopod extension dynamics. (*A*) A comparison [by differential interference contrast (DIC)] of RAW 264.7 macrophages undergoing frustrated phagocytosis on IgG (*Upper*) and BSA (*Lower*) opsonized glass surfaces (Movie S1). (*B*) Kymograph of the cell on the IgG-opsonized cell in *A*. (*C*) Contact area as a function of time for the cells in *A* (IgG, red; BSA, blue). (*D*) Example of the membrane folds quantification. Blue indicates the relative value (from the lowest point) of the membrane fluorescence from a portion of the cell basal membrane (from Fig. 1 *A* and *D* and Movie S2). Red indicates the cell-spreading area. The value of the membrane area lost from the buffer is clearly anticorrelated with the increase in spread area. In this example, the amount of membrane contained in folds should be estimated at around 40% of the original plasma membrane area; quantifications for 13 cells are in the main text. (*E*) Tether forces during cycles of protrusion, peak (T), and subsequent retraction during early P2. $n = 12$ cells.

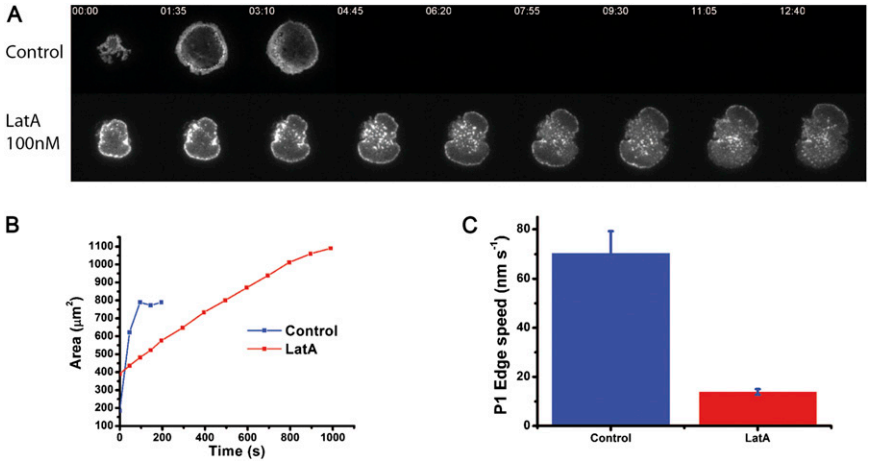

Fig. S2. Effect of the latrunculin A treatment on cell spreading. (*A*) Actin behavior in control (*Upper*) or latrunculin A-treated (*Lower*) cells. The spreading is about 4× slower for the lactrunculin-treated cell. (*B*) Spread area in function of time for the cells presented in *A*. (*C*) Quantification of the radial speed of the pseudopod extension in P1 for control and latrunculin A-treated cells (n = 20 cells for each case).

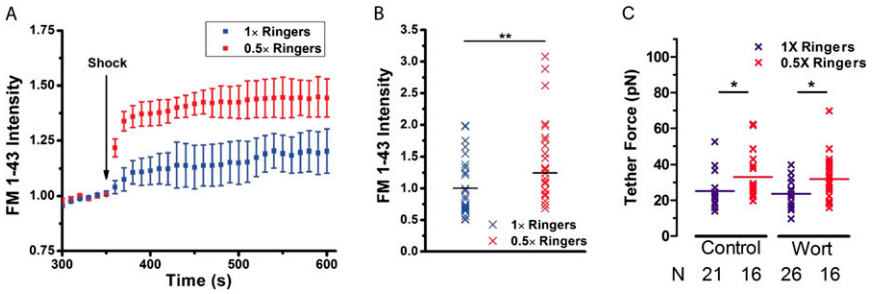

Fig. S3. Hypotonic shock increases plasma membrane area and increases membrane tension. (*A*) N-(3-triethylaminoniumpropyl)-4-(4-(dibutylamino) styryl) pyridinium dibromide (FM1-43) intensity (normalized to time of shock) of cultured, nonphagocytosing macrophages as a function of time during isotonic (1× Ringer's) or hypotonic (0.5× Ringer's) media replacement (maintaining FM 1–43). (*B*) FM 1–43 intensity for cultured macrophages imaged at 4 °C to block endocytosis and exocytosis following isotonic (1× Ringer's) or hypotonic (0.5× Ringer's) media replacement. (*C*) Membrane tension measurement (tether forces) in control or wotmannin-treated cells before and after hypotonic shock.

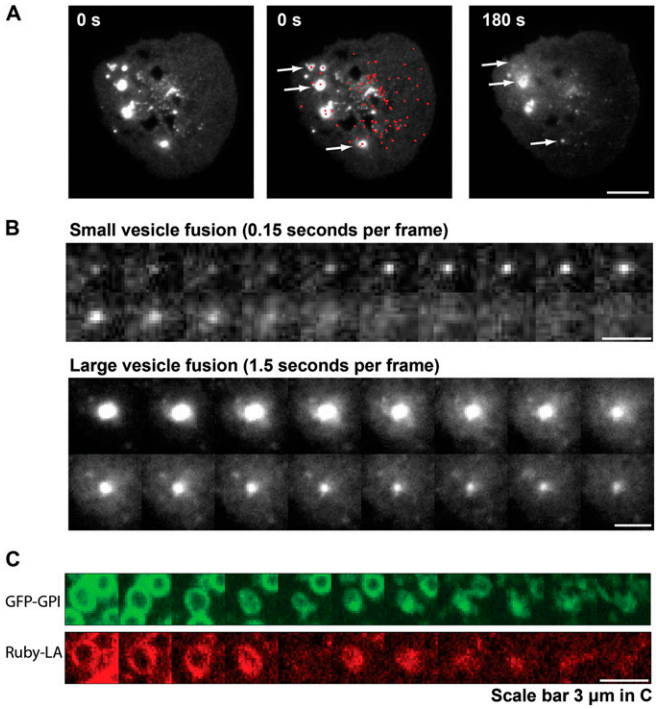

Fig. S4. Exocytosis of a GPI protein-rich compartment. (*A*) Distribution of GPI-GFP vesicles observed with total internal reflection fluorescence (TIRF) illumination following quenching of external fluorescence (red dots in the *Center* indicate location of fusion events between 0 and 180 s). (Scale bar, 10 μm.) (*B*) Fusion of small (*Upper*) and large (*Lower*) vesicles observed by TIRF. (Scale bars, 10 μm.) (*C*) Spinning-disk confocal microscopy of GPI-GFP and F-actin distribution during frustrated phagocytosis showing a vesicle shrinking with an actin coat as was observed for plasma membrane (PM)-GFP. (Scale bar, 3 μm.)

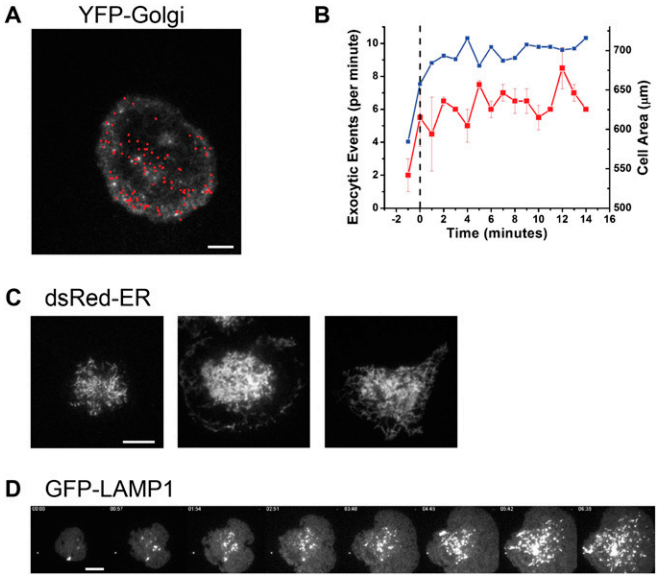

Fig. S5. The contribution of Golgi, lysosomal associated membrane protein 1 (LAMP1), and endoplasmic reticulum (ER) during pseudopod extension. (*A*) Location of Golgi exocytic events, indicated by red dots, observed over 15 min. (*B*) Quantification of Golgi exocytosis. Dotted line indicates time of transition (abscissa origin). (*C*) Several examples of ER distribution shown by red fluorescent protein from Discosoma sp. (dsRed)-ER during frustrated phagocytosis. (*D*) LAMP1 distribution during pseudopod extension.

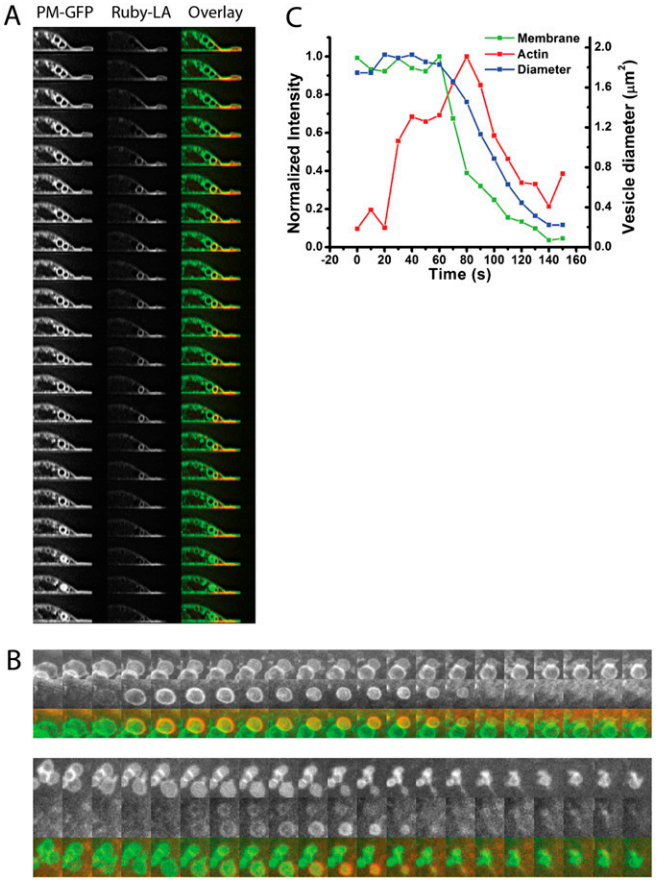

Fig. S6. Vesicles fuse following the transition in an actin-dependent manner. (*A*) Side view showing PM-GFP (green), Ruby-Lifeact (Ruby-LA) (F-actin, red), and overlay through a cross-section of a cell. The vesicle adjacent to the ventral membrane recruits an actin coat and shrinks in size (10 s per frame). (*B*) Upper view (from the top of the cell) of two examples of vesicles recruiting actin coats and fusing with the ventral plasma membrane. (*C*) Quantification of integrated intensity of membrane and actin and diameter for the vesicle in Fig. 3 *G* and *H* and Fig. S4*B* (*Lower*) during shrinkage.

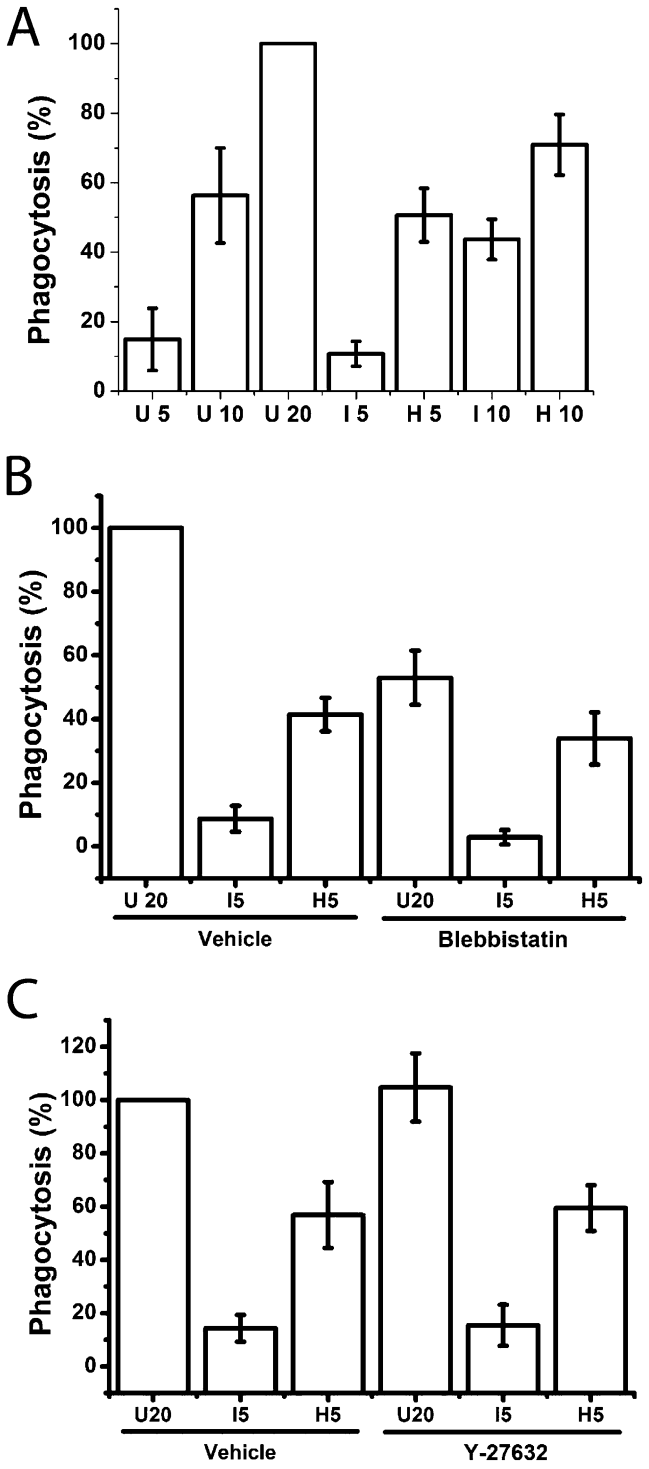

Fig. S7. Hypotonic shock increases phagocytic efficiency independently of MyosinIIA-mediated contractility. (*A*) Time course of phagocytosis and hypotonic shock. H, hypotonic; I, isotonic; U, unshocked; 5, 10, and 20 indicate the time period of ingestion in minutes at 37 °C before fixation. (*B*) Effect of blebbistatin (50 μM) on phagocytosis efficiency with hypotonic shock. (*C*) Effect of the Y-27632 compound (20 μM) on phagocytosis efficiency with hypotonic shock.

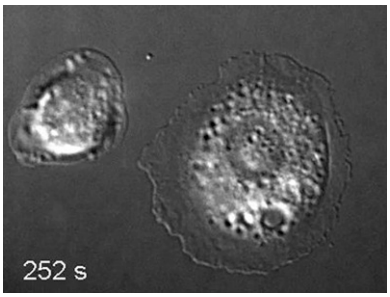

Movie S1. Pseudopod extension during frustrated phagocytosis observed with DIC microscopy (Fig. S1).

Movie S1

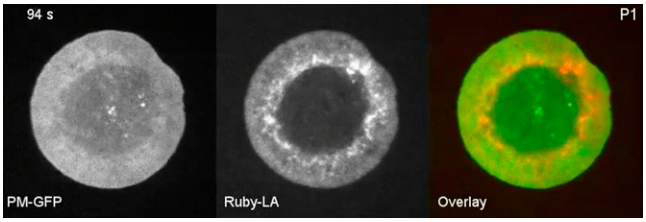

Movie S2. PM-GFP and Ruby-Lifeact distribution on the ventral surface during frustrated phagocytosis (Fig. 1 *A*, *B*, and *D*).

Movie S2

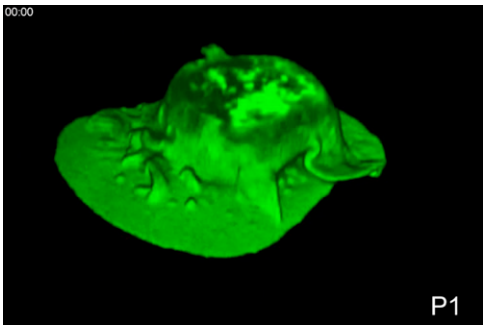

Movie S3. Three-dimensional reconstruction of PM-GFP during frustrated phagocytosis (Fig. 1*E*).

Movie S3

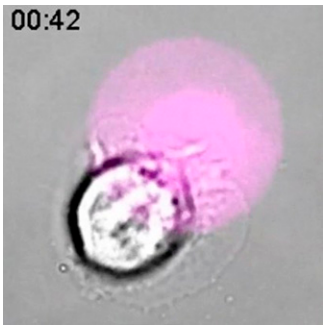

Movie S4. Membrane tether held through transition during frustrated phagocytosis (Fig. 2*A*).

Movie S4

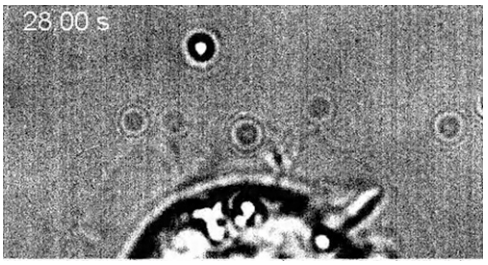

Movie S5. Frustrated phagocytosis on a 30-μm diameter circle of IgG (Fig. 2*B*).

Movie S5

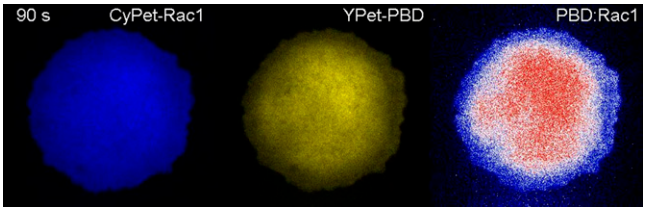

Movie S6. Cyan fluorescent protein coupled with Rac1 (CyPet-Rac1), yellow fluorescent protein coupled with the p21-activated protein kinas binding domain (YPet-PBD), and activation ratio through the transition (Fig. 2 *C* and *D*).

Movie S6

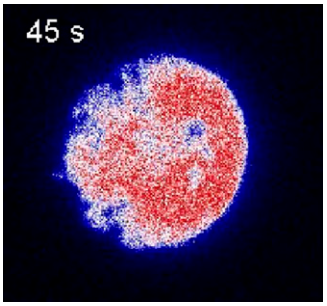

Movie S7. Protein Kinase AKT pleckstrin homology domain coupled with GFP (GFP-Akt-PH) through the transition (Fig. 2*E*).

Movie S7

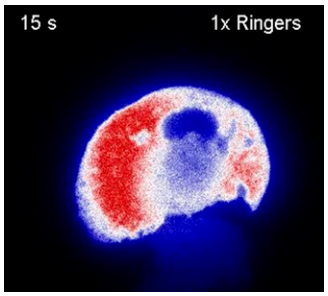

Movie S8. Stall of CyPet-Rac1 and YPet-PBD by hypotonic shock (Fig. 2*F*).

Movie S8

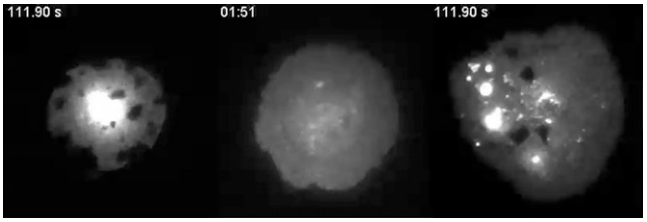

Movie S9. GPI-GFP exocytosis of three cells through the transition (Fig. 3 *E* and *F*).

Movie S9

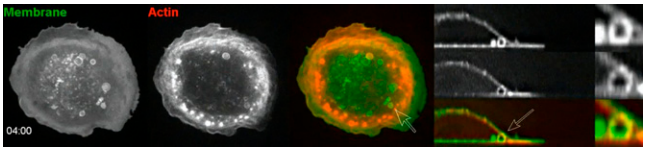

Movie S10. Fusion of large PM-GFP vesicles on recruitment of actin (Fig. 3 *G* and *H*).

Movie S10

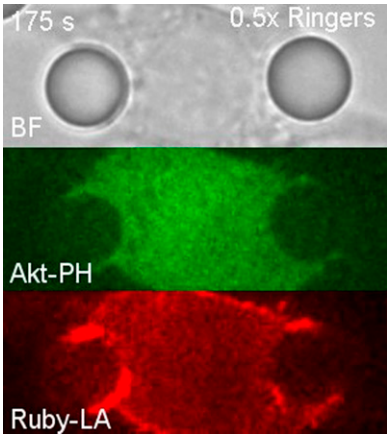

Movie S11. Tension-induced phagocytosis in the presence of 100 nM wortmannin (Fig. 4*D*).

Movie S11